Springer

Acta Mechanica Sinica

CrossMark click for updates

• RESEARCH PAPER •

Acta Mech. Sin., Vol. 40, 423608 (2024)
https://doi.org/10.1007/s10409-024-23608-x

New type of overrunning clutch based on curved-plate compression-torsion metamaterial

Yanbin Wang, Haifeng Ou, and Lingling Hu*

School of Aeronautics and Astronautics, Sun Yat-sen University, Shenzhen 518107, China

Received December 8, 2023; accepted March 1, 2024; published online June 12, 2024

Overrunning clutches are unidirectional drive mechanisms that are widely used in transmission systems. However, existing overrunning clutches have complex structures, require high preparation accuracy, and fail after a certain degree of wear. To address these issues, we propose a new type of overrunning clutch consisting of a conical structure and novel compression-torsion conversion (CTC) metamaterial with curved plates. Theoretical calculations are employed to guide the material distribution and ensure the deformation coordination of the curved-plate CTC metamaterial for greater ultimate torque. The transmission mechanism of the proposed overrunning clutch is derived to guide the parameter selection of the CTC metamaterial and the conical structure. Experiments and finite element simulations reveal that the curved-plate CTC metamaterial features excellent CTC efficiency, flexibility, and transverse stiffness, which is conducive reducing the resistance of the overrunning state and ensures stability during operation. The unidirectional transmission system constructed with the new overrunning clutch shows reliable performances under working and overrunning states. The constructed overrunning clutch provides an effective one-way transmission method. The clutch with simple construction and self-compensated ability for wear exhibits great potential in miniaturized and lightweight equipment or robots.

Overrunning clutch, Mechanical metamaterial, Compression-torsion conversion, Curved-plate configuration

Citation: Y. Wang, H. Ou, and L. Hu, New type of overrunning clutch based on curved-plate compression-torsion metamaterial, Acta Mech. Sin. 40, 423608 (2024), https://doi.org/10.1007/s10409-024-23608-x

1. Introduction

Overrunning clutches are widely used in civil traffic (bicycles, motorbikes, electric cars, etc.), the robot [1], the drive systems of helicopters [2], and many other aspects. The typical overrunning clutches are ratchet type [3,4], roller type [5-7] and sprag type [2,8,9]. However, the traditional structures are in discrete contact at multiple places and will not work after a certain degree of wear and tear. The traditional structures are process-sensitive multi-component assembled which increases the manufacturing cost and failure probability.

Mechanical metamaterials have brought unique properties that are rarely observed in natural materials, such as negative Poisson's ratio [10-13], negative stiffness [14,15], and negative thermos expansion [16]. The counterintuitive properties are derived from the well-designed configuration of their micro-structures. In industry, conversions between displacement and rotation are usually realized by using mechanical constructions [17,18], and the development of metamaterial has led to a completely new approach to compression-torsion conversion (CTC). Frenzel et al. [19] were the first to demonstrate the CTC metamaterial, and the conversion is realized through elastic deformation. The extraordinary property might lead to potential applications in transmission.

The proposed CTC metamaterials are mainly categorized into array type [20-22] and cylindrical shell type [23-25]. Fu et al. [20] proposed array type CTC metamaterial constructed of chiral unit cells. The buckling behavior of the slender array type CTC metamaterial is investigated [26]. Frenzel et al. [27] realized the CTC behavior of the array type metamaterial with a large unit cell number. Qiu et al.

*Corresponding author. E-mail address: hulingl@mail.sysu.edu.cn (Lingling Hu)
Executive Editor: Yuli Chen

[28] investigated the static mechanical properties of the array type CTC metamaterial constructed of the chiral unit cell. The CTC can be realized via a specific range of cross-frustum metamaterials [10]. Wei et al. [29] studied the energy absorption performances of the array type CTC metamaterial. Xu et al. [30] proposed an array type metamaterial with tunable CTC property. For energy absorption, a DNA-like CTC metamaterial is designed based on a friction mechanism [22]. The CTC behavior of the chiral metamaterial indicates prospects in dynamic and vibration control [25,31,32].

Zhang et al. [33] designed a cylindrical shell type CTC metamaterial constructed of bi-material unit cells. By using topology optimization, bi-material cylindrical shell type and beam CTC metamaterials were derived [34]. Based on the cylindrical shell type CTC metamaterial composed of handed shearing unit cells, Lipton et al. [35] proposed an actuator and stiffness adjustment structure. The curved beam structure exhibits better CTC properties than the inclined straight beam structure [36]. Based on the tape springs, a cylindrical shell type CTC metamaterial with multistability was proposed [37]. Hao et al. [38] conducted the ball passing test of a cylindrical shell type CTC metamaterial.

The array type CTC metamaterial can be freely dimensioned, but the transverse constraint limits the conversion property when the array number is large [27]. Cylindrical shell type CTC metamaterial features a centrosymmetric deformation mechanism but low space utilization [39,40], and the metamaterial features low stiffness under transverse load. Curved-plate CTC metamaterial [23] was proposed based on the mechanical analysis of the inclined beam cylindrical shell type CTC metamaterial, while the calculations feature large errors derived from the curl during modeling.

In this article, a new type of overrunning clutch constructed of the CTC metamaterial and a conical surface friction structure is designed. To enhance the ultimate bearing capacity of the CTC metamaterial, a spatial expansion method is proposed in this article. Then both bi-beam CTC metamaterial and curved-plate CTC metamaterial with accurate geometrical configurations are derived based on the built theoretical model. The proposed bi-beam CTC metamaterial features higher bearing capacity and unison conversion efficiency. Furthermore, the experiments and finite-element simulations reveal that the proposed curved-plate CTC metamaterial features excellent CTC efficiency, better transverse stability, and enhanced bearing capacity. The driving and overrunning are realized through the combination of the CTC metamaterial and the conical surface friction structure, and the transmission mechanisms are investigated theoretically. A one-way transmission system is constructed based on the proposed overrunning clutch.

2. Modeling of the curved-plate metamaterial

To enhance the bearing capacity of the original inclination beam CTC metamaterial, the material volume of the original configuration needs to be increased. However, the arbitrary addition of material will make the deformation incongruous. To solve this problem, a deformation-coordinated structural configuration is proposed while maintaining excellent CTC properties.

The original inclination beam CTC metamaterial is exhibited in Fig. 1(a). Force or torque is applied on the upper plate, and the lower plate is fixed. Δz, Δx, and $\Delta\varphi$ represent the displacement of point B along the vertical, horizontal, and circumferential directions. H, R, and d denote the height of the inclination beam, the radius of the metamaterial, and the diameter of the circular cross-section of the inclination beam. W is defined as half the length of the projection of the inclination beam onto the x-y plane, while T represents the distance between the projection of the inclination beam and the center of the circle. The inclination beam is established from point A ($x = -W$, $y = T$) to point B ($x = W$, $y = T$). It is assumed that point B moves perpendicular to the beam, and the upper circular ring is undeformed. When the metamaterial is compressed, the torsion angle can be expressed as

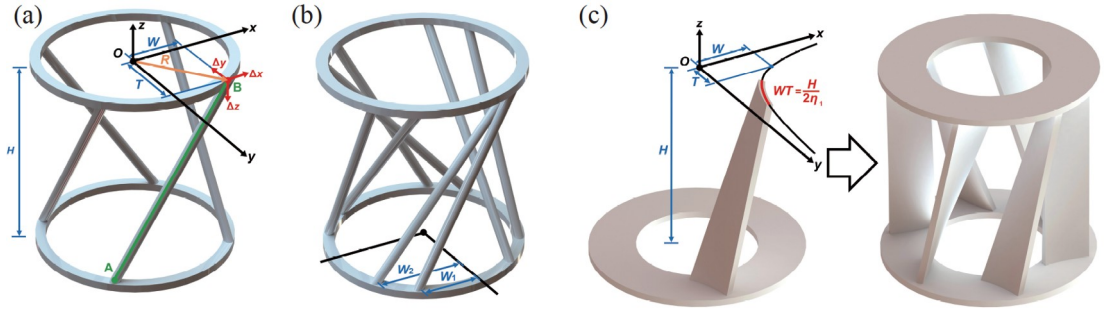

Figure 1 (a) Original CTC metamaterial constructed of inclination beam. (b) Bi-beam CTC metamaterial with unison conversion efficiencies. (c) Construction of the curved-plate CTC metamaterial.

$$\alpha_1 = \Delta x_1 \frac{R}{\sqrt{R^2 - W^2}} \frac{1}{R} = \Delta z_1 \frac{H}{2W\sqrt{R^2 - W^2}}, \tag{1}$$

where α_1 represents the torsion angle of the upper plate under compression. The CTC efficiency is defined as the ratio of torsion angle to displacement under compression load, and the torsion-displacement conversion (TDC) efficiency is defined as the ratio of displacement to torsion angle under torsion load. The CTC efficiency of the inclination beam at a certain radius R can be expressed as

$$\eta_1 = \frac{\alpha_1}{\Delta z_1} = \frac{H}{2W\sqrt{R^2 - W^2}} = \frac{H}{2WT}, \tag{2}$$

where $T^2 = R^2 - W^2$.

Under torsion, the displacement can be expressed as

$$\Delta z_2 = \frac{2W}{H} \Delta x_2 = \frac{2\alpha_2 W\sqrt{R^2 - W^2}}{H}, \tag{3}$$

where α_2 denotes the applied torsion angle on the upper plate. The TDC efficiency can be expressed as

$$\eta_2 = \frac{\Delta z_2}{\alpha_2} = \frac{2W}{H}\sqrt{R^2 - W^2} = \frac{2WT}{H}. \tag{4}$$

From Eqs. (2) and (4), it can be derived that

$$\begin{aligned} &\frac{\alpha_1}{\Delta z_1} = \frac{H}{2W\sqrt{R^2 - W^2}} \geqslant \frac{H}{R^2}, \\ &\frac{\Delta z_2}{\alpha_2} = \frac{2W\sqrt{R^2 - W^2}}{H} \leq \frac{R^2}{H}. \end{aligned} \tag{5}$$

The results reveal that the metamaterial with $W = T$ exhibits the lowest CTC efficiency η_1 and the highest TDC efficiency η_2, and the TDC efficiency always decreases when the CTC efficiency increases, since $\eta_1 \cdot \eta_2 = 1$. Moreover, to obtain certain efficiency η_1, there are usually two solutions W_1 and W_2, and the following relationship exists:

$$W_2 = \sqrt{R^2 - W_1^2} = T_1. \tag{6}$$

So bi-beam CTC metamaterial with unison CTC efficiency can be derived as shown in Fig. 1(b). The metamaterial is constructed of two kinds of beams ($W_1 = T_2$). Points on the upper plate ($x_1 = W_1, y_1 = T_1; x_2 = T_1, y_2 = W_1$) and the lower plate ($x_3 = -W_1, y_3 = T_1; x_4 = -T_1, y_4 = W_1$) are linked to establish two inclination beams. The capacity of the original CTC metamaterial can be enhanced through the bi-beam design.

To construct inclination beams with the same CTC or TDC efficiencies at different radiuses, it can be obtained from Eqs. (2) and (4) that

$$WT = \frac{H}{2\eta_1}, \quad WT = \frac{H\eta_2}{2}. \tag{7}$$

The calculation reveals that any inclination beam constructed along the above inverse proportional curve features unison CTC and TDC efficiencies. Therefore, curves are set on the upper plate ($WT = 0.5H/\eta_1$) and the lower plate ($WT = -0.5H/\eta_1$). Consequently, the curved-plate is established by connecting two curves, as shown in Fig. 1(c). The proposed metamaterial features harmonized CTC efficiency and coordinated deformation.

3. Mechanical properties of the curved-plate metamaterial

3.1 CTC efficiency of the curved-plate metamaterial

To study the mechanical properties of the bi-beam and curved-plate CTC metamaterial, linear finite-element simulations are conducted in the software ABAQUS. 8-node hexahedral solid (C3D8R) elements are used in the simulations, and the material properties are defined according to the material for the experiment (Young's modulus E = 1875 MPa, Poisson's ratio v = 0.4). Simulations are conducted to verify the simplified mechanical calculation method. A reference point is attached to the upper plate. The lower end is fixed, and the compression or torsion displacement is applied on the reference point (U_3 = 1 mm or $UR_3 = 1°$, $U_1 = U_2 = UR_1 = UR_2 = 0$).

The simplified calculation predicts the CTC/TDC efficiency of the original inclination beam CTC metamaterial precisely when the inclination beam is thin (R = 30 mm, H = 60 mm, d = 3 mm), as shown in Fig. 2(c). The theoretical calculation is derived from Eq. (2). Numerical models of bi-beam CTC metamaterials with R = 30 mm, H = 60 mm, and d = 3 mm are established, and the simulation results are shown in Fig. 2(c). The length W_1 has opposite effects on the CTC and TDC efficiencies of the bi-beam metamaterial. When W_1 approaches $R/\sqrt{2}$, two beams will interfere with each other. Two groups of simulation agree well with the theoretical calculations. Under compression of 1 mm, Von Mises stress distributions of the inclination beam CTC metamaterial with W = 20 mm and the bi-beam CTC metamaterial with W_1 = 15 mm are exhibited in Fig. 2(a) and (b). The results indicate that the local stresses in the metamaterials are acceptable under not too large displacement loads. The validity of the calculations and the feasibility of the bi-beam configuration are verified.

Models of curved-plate CTC metamaterials with R = 30 mm, H = 60 mm, and width of curved-plate equals 2 mm are established as shown in Fig. 3(a) and (d) (models with η_1^* = 5°/mm and η_1^* = 15°/mm). Mesh size is set as 0.5 mm (1/4 of the thickness of the curved-plate) to ensure the accuracy of the finite-element simulations. Figure 3(b) and (e) exhibit the Von Mises stress distributions of the curved-plate CTC metamaterials under compression of 5 mm. The stress distributions of the metamaterial under torsion of 20° are exhibited in Fig. 3(c) and (f). The metamaterial with

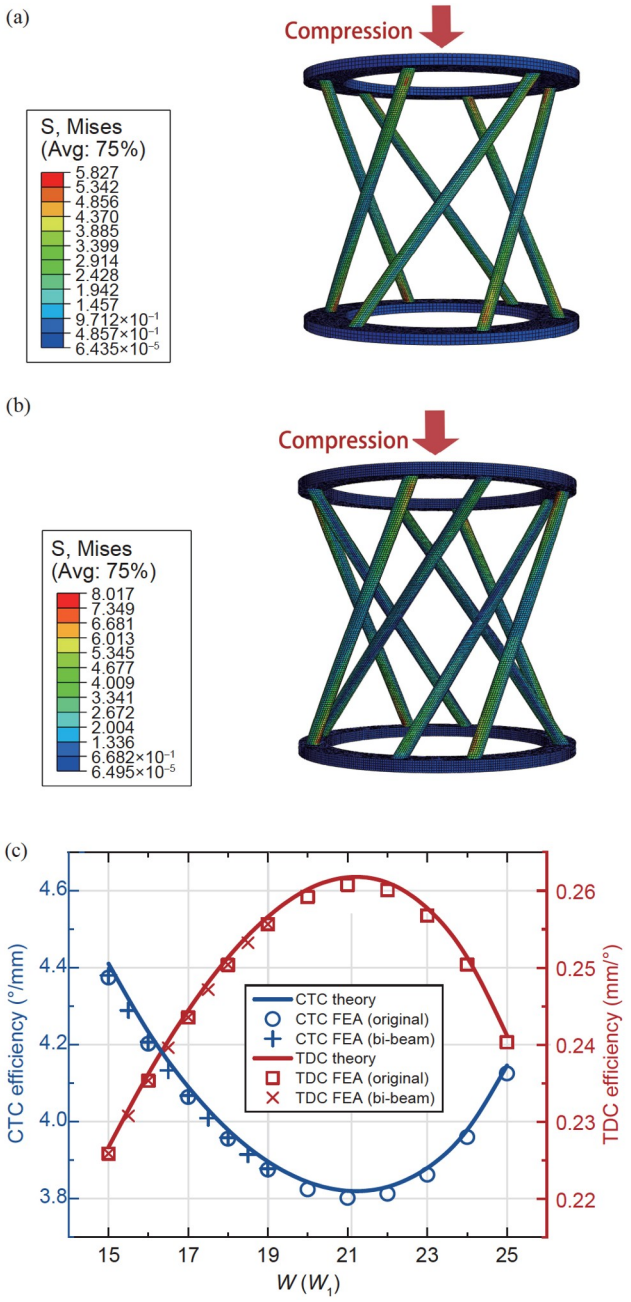

Figure 2 Finite-element simulations of the inclined beam and bi-beam CTC metamaterials. (a) Von Mises stress distributions of the inclination beam CTC metamaterial with W = 20 mm under compression. (b) Von Mises stress distributions of the bi-beam CTC metamaterial with W_1 = 15 mm under compression. (c) Effects of length W on the conversion efficiencies of the original CTC metamaterial and effects of length W_1 on the conversion efficiencies of the bi-beam CTC metamaterial.

straighter curved-plates exhibits larger η_1 and lower η_2. Figure 4 exhibits the theoretical and finite-element results of the curved-plate metamaterial with different η_1^* (the curved-plate is constructed according to $WT = 0.5H/\eta_1^*$). The theoretical results are derived from Eq. (7). Figure 5(a) and (b) exhibit the effects of displacement/torsion angle on the CTC/TDC efficiency. The η_1 decreases when the displacement increases, and the η_2 increases when the torsion angle increases. The metamaterial with a smaller η_1^* exhibits more stable conversion efficiencies. The calculations and finite-element simulations are in good agreement, indicating that the deformations of the metamaterials are coordinated. The bi-beam and curved-plate configurations can improve the bearing capacity of the original CTC metamaterial without damaging the CTC performance.

3.2 Flexibility coefficients of the curved-plate metamaterial

In this section, the flexibility of the proposed curved-plate metamaterial is investigated. The relationship between displacement, force, torsion angle, and torque can be expressed as

$$\begin{pmatrix} s_1 & s_c \\ s_c & s_2 \end{pmatrix}\begin{bmatrix} F \\ T \end{bmatrix} = \begin{bmatrix} \Delta \\ \varphi \end{bmatrix}, \tag{8}$$

where s_1, s_2, and s_c represent the flexibility coefficients, F and T represent the reaction force and reaction moment of the reference point under compression or torsion. The flexibility matrix of the curved-plate CTC metamaterial is derived from the finite-element simulations under the boundary condition as shown in Fig. 3(b) and (c). Yang et al. [41] gave the expression of the stiffness matrix, and the stiffness matrix equals the inverse of the flexibility matrix.

$$\begin{pmatrix} k_1 & k_c \\ k_c & k_2 \end{pmatrix} = \begin{pmatrix} \dfrac{s_2}{s_1 s_2 - s_c^2} & \dfrac{-s_c}{s_1 s_2 - s_c^2} \\ \dfrac{-s_c}{s_1 s_2 - s_c^2} & \dfrac{s_1}{s_1 s_2 - s_c^2} \end{pmatrix}. \tag{9}$$

The flexibility coefficients are derived from the simulation results as shown in Fig. 6(b)-(d). When $\eta_1^* > 8°/\text{mm}$, take the middle section of the curve with 15 mm $\le R \le$ 25 mm. When $\eta_1^* \le 8°/\text{mm}$, the curve has no point of intersection with R = 15 mm, so half of the curve plate is preserved. Figure 6(a) exhibits the effect of the η_1^* on the volume of the curved-plate (not including the upper and lower circular plate), and the metamaterial with η_1^* = 8°/mm features the maximum volume. When η_1^* increases, the included angle between the curve plates and the compression direction becomes smaller, and the s_1 decreases as shown in Fig. 6(b). The metamaterial with η_1^* = 8°/mm features minimum s_2 as exhibited in Fig. 6(c). The flexibility coefficient s_c derived from compression and torsion loadings is proven the same by using a reciprocal theorem, and the conclusion is confirmed by the simulations. With the increases of η_1^*, the coupling coefficients s_c decreases, as shown in Fig. 6(d).

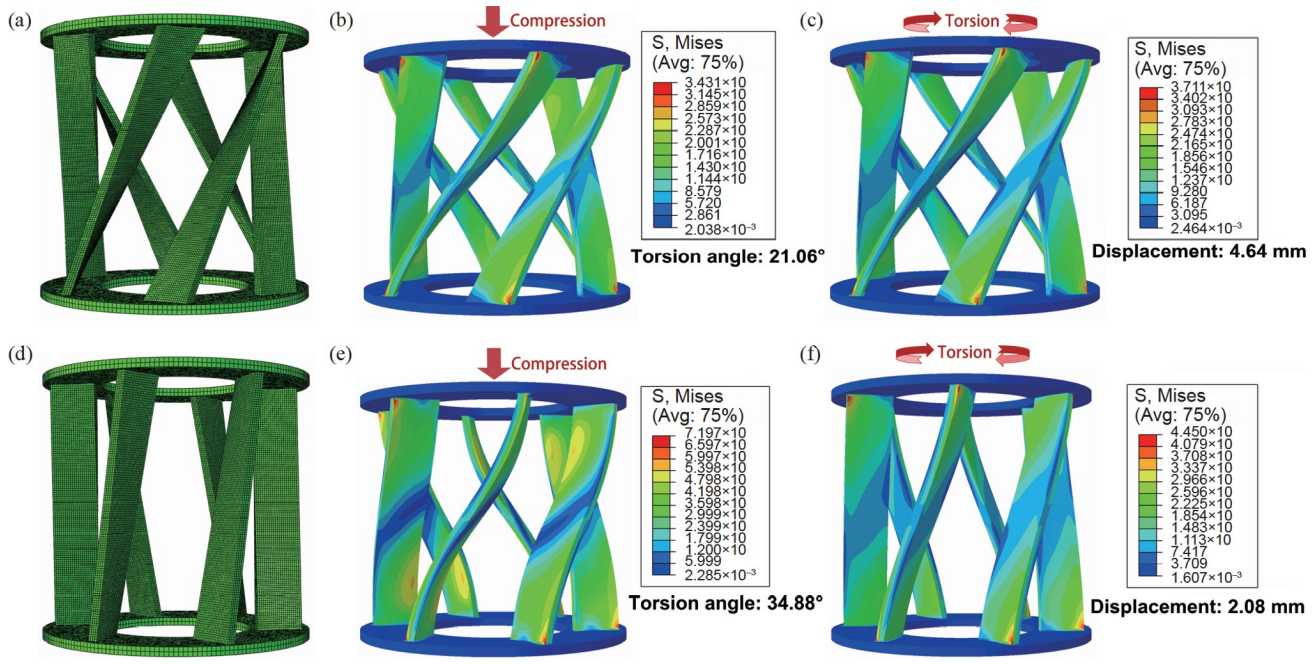

Figure 3 Finite-element simulations of the curved-plate CTC metamaterial. (a) Mesh generation and Von Mises stress distributions of the metamaterial with $\eta_1^* = 5°/\text{mm}$, (b) under compression of 5 mm, and (c) under torsion of 20°. (d) Mesh generation and Von Mises stress distributions of the metamaterial with $\eta_1^* = 15°/\text{mm}$, (e) under compression of 5 mm, and (f) under torsion of 20°.

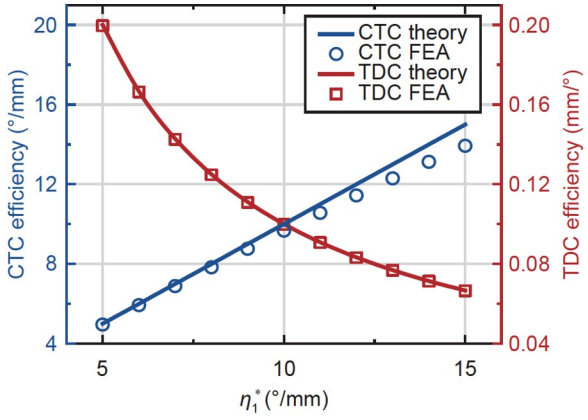

Figure 4 Effects of η_1^* on the CTC and TDC efficiencies of the curved-plate CTC metamaterial.

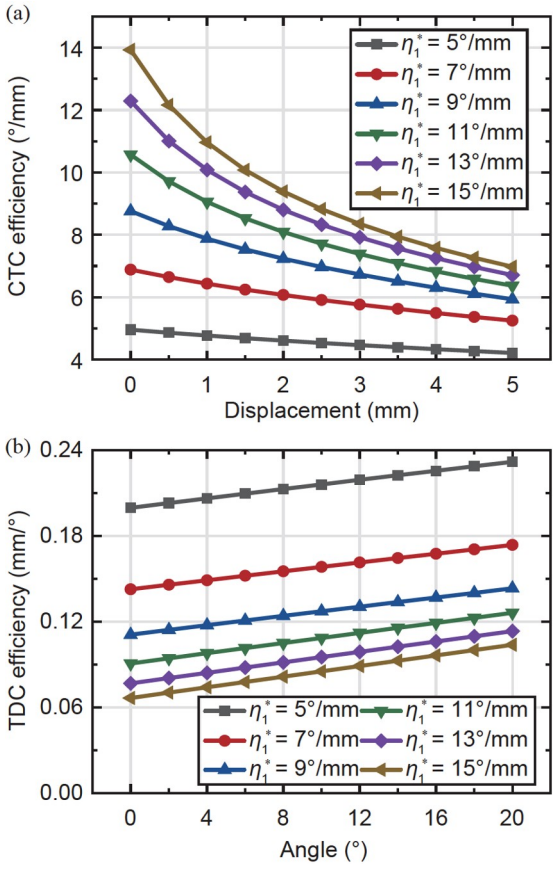

Figure 5 Geometric nonlinear behaviors of the curved-plate CTC metamaterial. (a) Effects of displacement on the CTC efficiency. (b) Effects of torsion angle on the TDC efficiency.

3.3 Transverse stiffness of the curved-plate metamaterial

Generally, the curved-plate metamaterial exhibits high stiffness. The curved-plate CTC metamaterials might feature higher stability than that of the original CTC metamaterial under non-ideal load. For comparison, the bending of the metamaterials under horizontal force is investigated, as shown in Fig. 7(a). The coefficient β is defined to illustrate the stability of the metamaterials.

$$\beta = \frac{F_h/\Delta_h}{F_v/\Delta_v}, \tag{10}$$

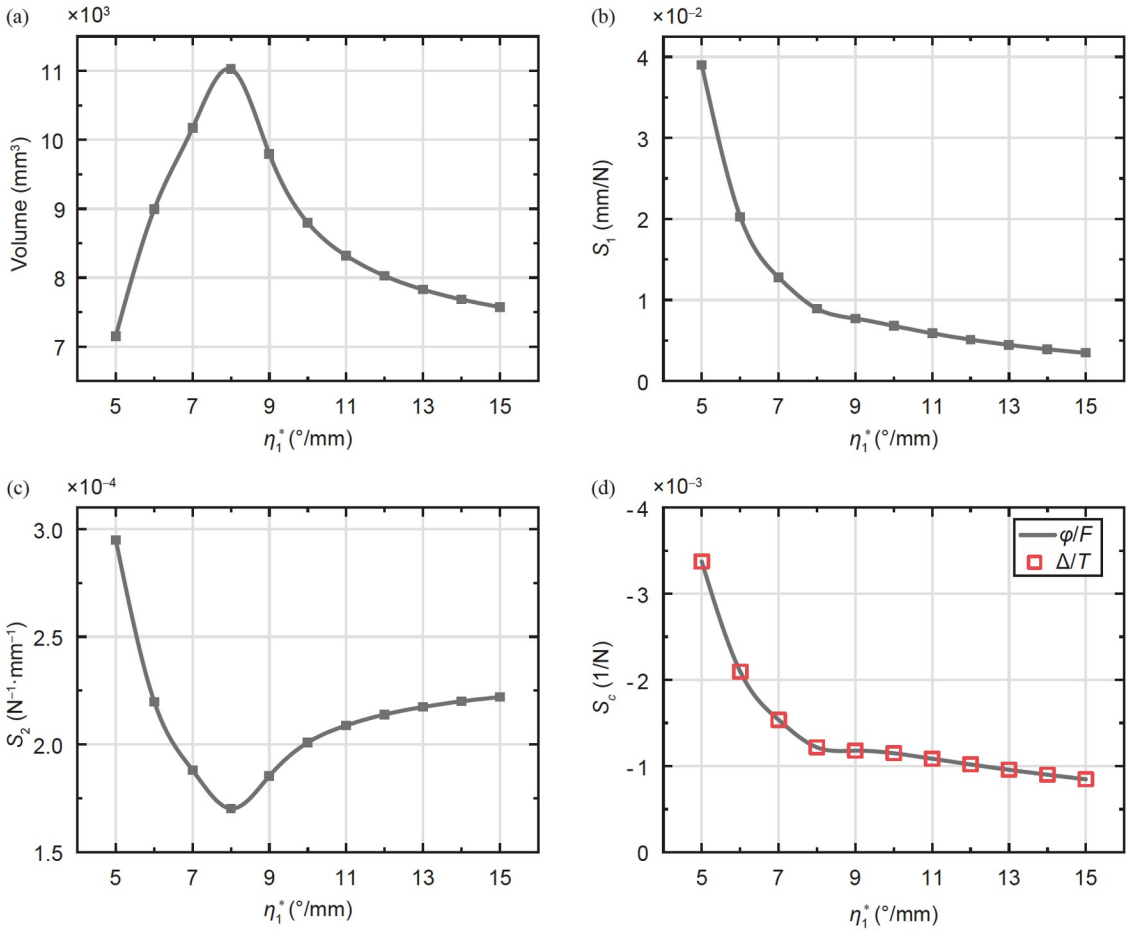

Figure 6 (a) Effects of η_1^* on the volume of the curved-plate. (b)-(d) Effects of η_1^* on the flexibility coefficients s_1, s_2 and s_c.

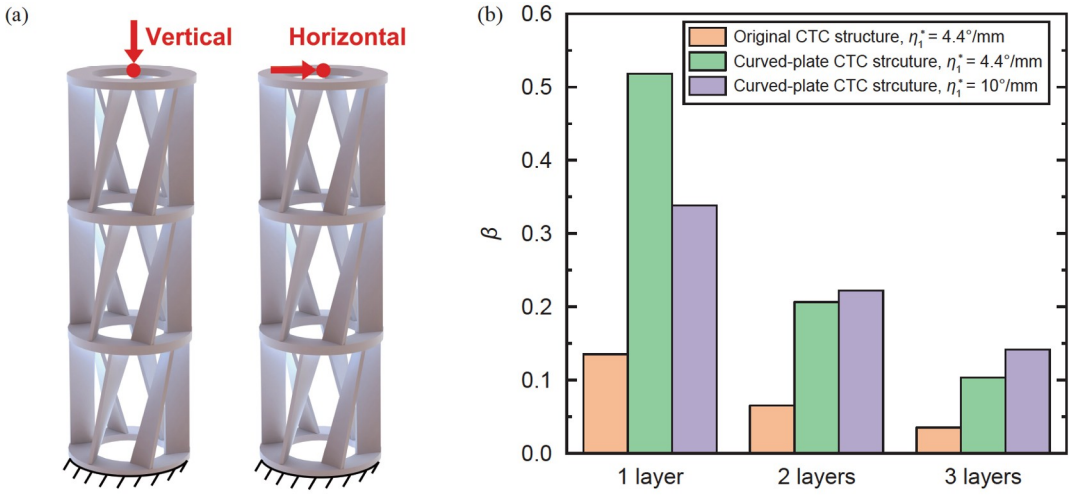

Figure 7 (a) Boundary conditions of vertical and horizontal loadings. (b) Coefficient β of inclination beam and curved-plate CTC metamaterials with different numbers of layers.

where F_h and F_v represent the horizontal and vertical forces, and the corresponding displacements are Δ_h and Δ_v. Figure 7(b) shows the coefficient β of the inclination beam and curved-plate CTC metamaterials with different numbers of layers. The deformation of the curved-plate is unison under working load (vertical direction), and the metamaterial exhibits high stiffness under unwanted load (horizontal direction).

3.4 Experiments of the curved-plate metamaterial

In this subsection, compression and torsion experiments are conducted to verify the theoretical and simulation results. Curved-plate metamaterial specimens with R = 30 mm, H = 60 mm, width of curved-plate equals 2 mm, η_1^* = 5°/mm, 7°/mm, 9°/mm, 11°/mm, 13°/mm, 15°/mm are manufactured for the experiments as shown in Fig. 8(a) and (b). The specimens for torsion experiments are in double layer mirror configuration (Fig. 8(b)). 3D printer Lite 600 is employed to manufacture the specimens, and the Young's modulus of the photopolymer resin is tested before the experiment (Somos® LEDO 6060, 1875 MPa). The CTC behavior of the metamaterial is derived from the geometrical configuration rather than the material's property. The metamaterial and the overrunning clutch can also be made of other materials, and this has little effect on their functions. In the present work, the specimens were 3D-printed with photopolymer resin to verify the design strategy, which is sufficiently accurate and inexpensive. Quasi-static compression experiments are conducted in the Instron compression testing machine (68TM-10) as shown in Fig. 9(a). Under compression, the lower plate is placed on a rotatable plate by a bearing, and a laser is fixed on the rotatable plate.

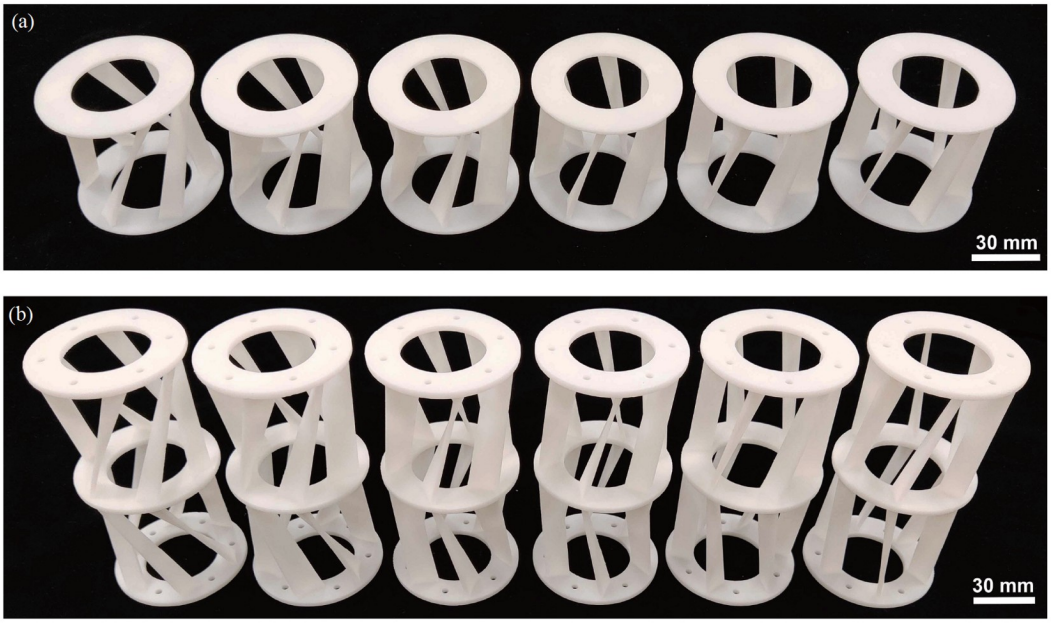

Figure 8 3D printing specimens for CTC (a) and TDC (b) efficiencies tests. Scale bar, 30 mm.

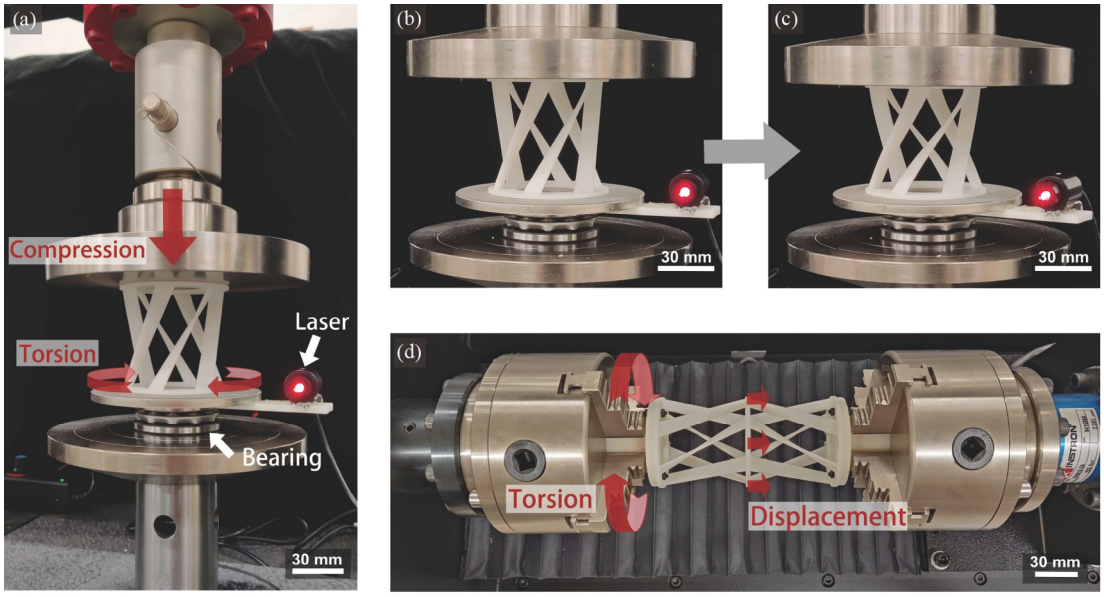

Figure 9 (a)-(c) Compression tests of the curved-plate CTC metamaterials. (d) Torsion tests of the curved-plate CTC metamaterials. Scale bar, 30 mm.

The upper plate of the specimen is in contact with the upper indenter with no relative sliding. As exhibited in Fig. 9(b) and (c), the torsion angle can be derived by measuring the movement of the laser light emitted at a board, and the CTC efficiency is calculated [42]. Quasi-static torsion experiments are conducted in the Instron torsion testing machine (MT2) as shown in Fig. 9(d). The rotation is applied on the left side of the double layer specimens, and the right side of the specimens is fixed. Under torsion, the torsion angle of two layers is the same, and the sum of the length changes of two layers equals zero due to its symmetry. The displacement of the middle plate is measured, and the TDC efficiency is derived. The experiments are in good agreement with the corresponding nonlinear finite-element simulation results, as shown in Fig. 10. The CTC efficiency features a higher nonlinearity when the η_1^* increases and the TDC efficiency changes less with different η_1^*.

4. Structural design of the new type of overrunning clutch

4.1 Theoretical calculations of the overrunning clutch

In virtue of the excellent bearing capacity and controllable flexibility of the curved-plate CTC metamaterial, it can be used for composing a new type of overrunning clutch. The driving and overrunning are realized through the combination of the curved-plate CTC metamaterial and the conical surface friction structure as exhibited in Fig. 11(a). The input shaft and the inner conical structure are connected. The curved-plate CTC metamaterial is connected to the outer conical structure and the output side. Axial displacements of the input shaft and the output side are constrained. Under driving torque, the CTC produces an axial force that compacts the conical structure. When the maximum frictionless torque is larger than the driving torque, the overrunning clutch is self-locking: there is no relative rotation between the conical surfaces, and the torque is transferred. Under overrunning torque, the CTC produces an axial force that separates the conical surfaces, and the torque is not transferred. Compared with the traditional overrunning clutch, the proposed structure is not process-sensitive, and the conical surface friction structure still works after wear and tear.

The flexibility coefficients of the CTC metamaterial are studied in the above section. Furthermore, the mechanical behaviors of the conical surface friction structure are investigated in this section. To begin with, the self-locking of the structure under driving load is needed. The blue element on the surface is considered, as shown in Fig. 11(b). The total torque T can be calculated as

$$T = \int r \mathrm{d}F_T. \tag{11}$$

Under the load of torque T, there is no axial strain of the CTC metamaterial in the x direction, and the axial force F_D is generated from the CTC behavior of the curved-plate metamaterial.

$$F_D = -\frac{s_c}{s_1} T = \eta_1 T, \tag{12}$$

where η_1 represents the ratio of force to torque of the CTC metamaterial under pure torsion, and the ratio equals the CTC efficiency of the structure. It is assumed that r takes a fixed value, and exists

$$\mathrm{d}F_D = \eta_1 r \mathrm{d}F_T. \tag{13}$$

In the x-y plane, the forces $\mathrm{d}F_N$, $\mathrm{d}F_D$, and $\mathrm{d}F_T$ are in equilibrium, exists

$$\mathrm{d}F_N = \frac{\mathrm{d}F_D}{\sin\theta} = \frac{\eta_1 r \mathrm{d}F_T}{\sin\theta}, \tag{14}$$

where θ represents the inclined angle of the conical surface, and the force of friction is generated,

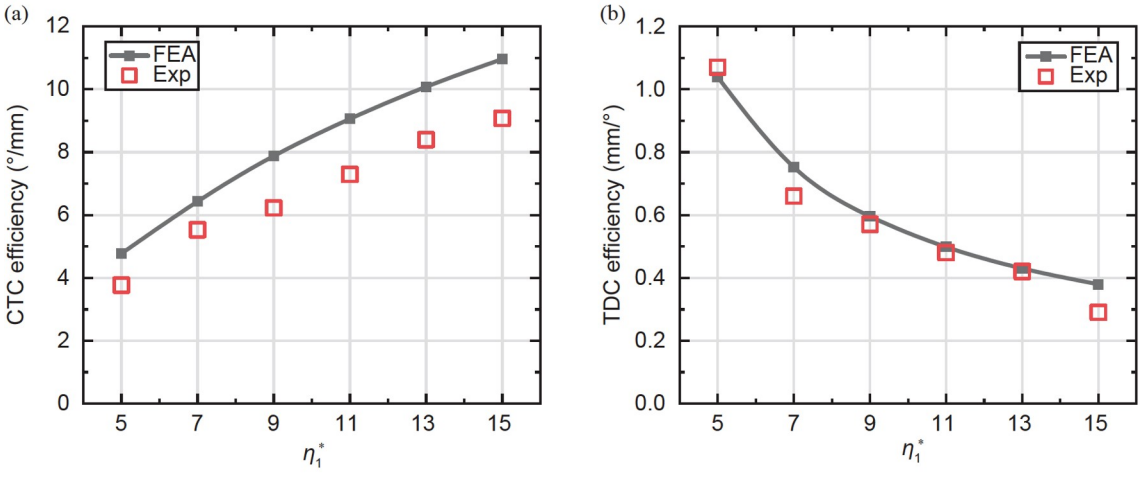

Figure 10 Comparison of finite-element simulations and experiments. (a) Effect of η_1^* on the CTC efficiency. (b) Effect of η_1^* on the TDC efficiency.

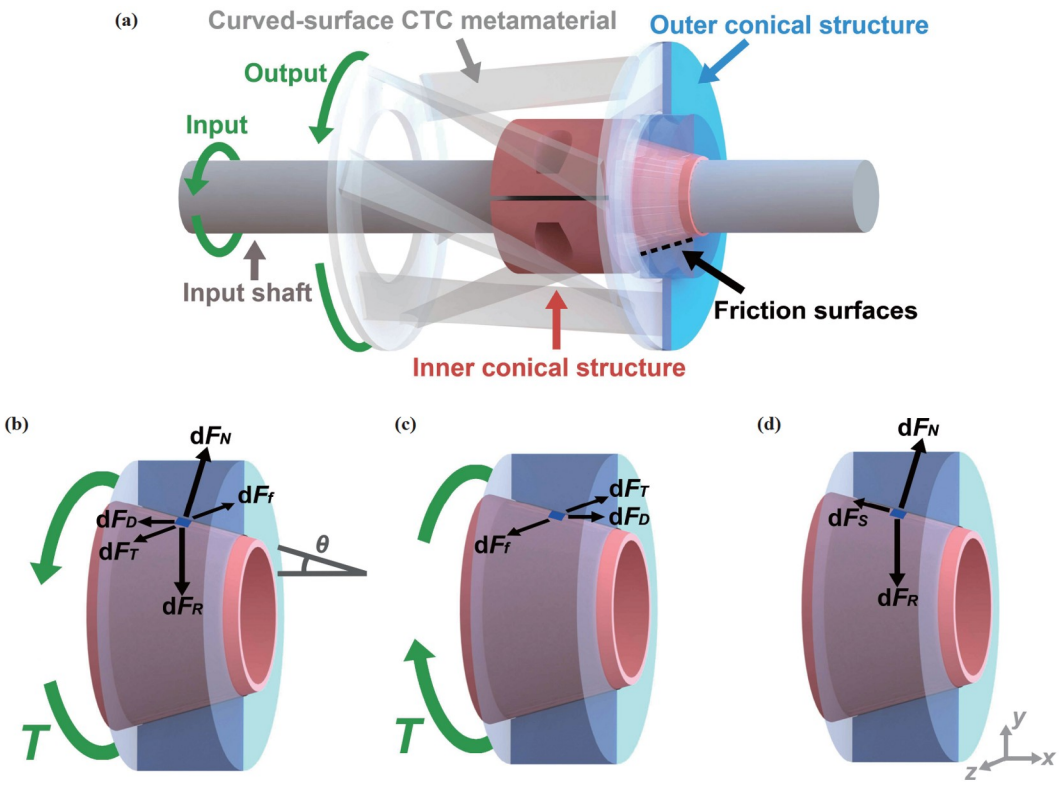

Figure 11 (a) Schematic diagram of the proposed overrunning clutch (axial displacements of the input shaft and the output side are constrained). Force analysis of the conical surface friction structure: (b) working state, (c) overrunning state, and (d) resting state.

$$\mathrm{d}F_f < \mu \mathrm{d}F_N = \frac{\mu\eta_1 r \mathrm{d}F_T}{\sin\theta}. \tag{15}$$

It is assumed that the maximum static friction factor equals the dynamical friction factor. If the allowable force of friction is larger than the shear force,

$$\mathrm{d}F_{f_{\max}} = \frac{\mu\eta_1 r \mathrm{d}F_T}{\sin\theta} > \mathrm{d}F_T, \tag{16}$$

$$\frac{\mu\eta_1 r}{\sin\theta} > 1, \tag{17}$$

the structure is self-locked when the inequality is satisfied.

Under reversed torque T in the opposite direction, the force $\mathrm{d}F_D$ is also reversed, the surface is separated, and the overrunning of the structure is realized (Fig. 11(c)).

The conical structure with a smaller angle has better self-locking ability. However, the jamming of the conical structure needs to be prevented. After driving, the deformation of the conical structure causes a radial force $\mathrm{d}F_R$ on the element surface, as shown in Fig. 11(d). The compression force $\mathrm{d}F_N$ led to a force of friction $\mathrm{d}F_S$, and the maximum static friction can be expressed as

$$\mathrm{d}F_{S_{\max}} = \mu \mathrm{d}F_N = \mu\cos\theta \mathrm{d}F_R. \tag{18}$$

If the maximum static friction is larger than the component of the $\mathrm{d}F_R$ parallel to the conical surface, the structure is jammed. To prevent the jamming, exist

$$\mathrm{d}F_S = \mathrm{d}F_R\sin\theta > \mathrm{d}F_{S_{\max}} = \mu\cos\theta \mathrm{d}F_R, \tag{19}$$

$$1 > \frac{\mu}{\tan\theta}. \tag{20}$$

In conclusion, the parameters should satisfy Eqs. (17) and (20) for the effective operation of the proposed overrunning clutch. The calculations reveal that larger η_1 and radius r provide better performance.

When the self-locking of the structure is realized, the CTC metamaterial with higher s_1 features lower resistance when overrunning, as shown in Fig. 6(b). In the following experiment, curved-plate CTC metamaterial with $\eta_1^* = 5°/\mathrm{mm}$ is employed to construct the overrunning clutch. The equivalent radius r is 12 mm, the inclined angle θ of the conical structure is 15°, and the friction coefficient is 0.25. Equations (17) and (20) are satisfied under the above conditions.

4.2 Construction of the one-way transmission system

Based on the above calculation, the curved-plate CTC metamaterial with $\eta_1^* = 5°/\mathrm{mm}$ and the conical friction surface structure with inclined angle $\theta = 15°$ are employed to construct the overrunning clutch. The overrunning clutch is constructed and arranged in a driving system, as shown in Fig. 12(a). Chain wheels and chains are set in the driving

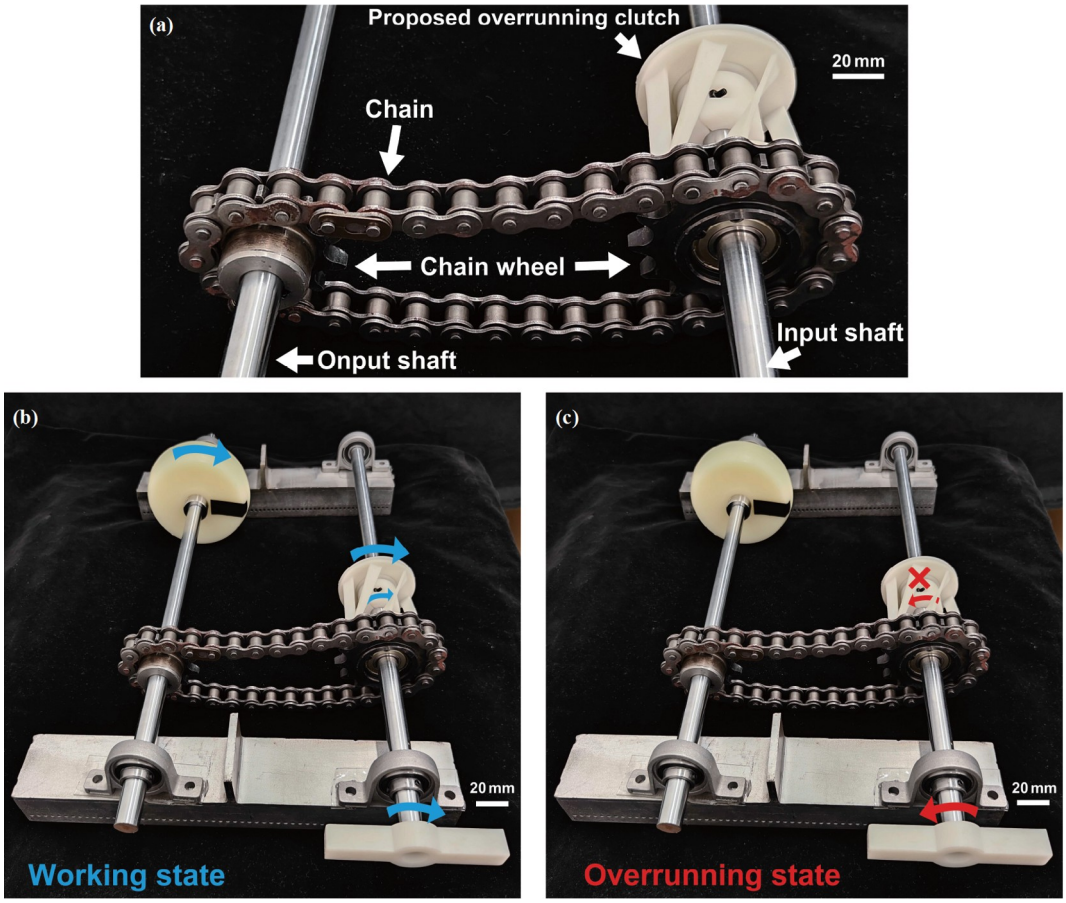

Figure 12 (a) Construction of the driving system; (b) the working state of the driving system; (c) the overrunning state of the driving system. Scale bar, 20 mm.

system for transmission. The inner conical structure is connected to the input shaft, and the outer conical structure is connected to the curved-plate CTC metamaterial. The input chain wheel is connected to the curved-plate metamaterial, and the output chain wheel is fixed on the output shaft. A bearing is set between the input chain wheel and the input shaft, so the relative rotation can occur, but the axial displacement is constrained. A driven wheel is fixed on the output shaft to increase the load and make the rotation more visual.

When rotating the input shaft clockwise, the overrunning clutch converts the rotation, and the driven wheel is rotated, as shown in Fig. 12(b). When the input shaft is rotated counterclockwise, overrunning is realized, and the following parts are not driven, as exhibited in Fig. 12(c). A rapid switch between the working state and the overrunning state can be realized. The constructed driving system is self-locked under the working state and exhibits lower resistance torque under the overrunning state. An innovative and reliable overrunning clutch design is presented.

Existing overrunning clutches are multi-component assembled, and the components are contacted at multiple discrete locations, which increases the probability of failure and maintenance costs. In comparison, the proposed overrunning clutch has a simple construction and the ability to compensate after wear. The friction of the proposed overrunning clutch occurs at the conical surface friction structure, where the two surfaces are in extensive contact and only require axial adjustment to continue transmission after heavy wear.

In this work, the proposed overrunning clutch is fabricated by 3D printing for principle experiments, thus the base material limits its ultimate load-bearing capacity. Besides, the simple design of the proposed structure is insensitive to precision, which makes it easy to manufacture on a small scale. Therefore, in our future work, we will carry out research on the miniaturization and high load-carrying capacity of the proposed overrunning clutch.

5. Conclusion

This study presents a new type of overrunning clutch consisting of curved-plate CTC metamaterial and the conical surface friction structure. The curved-plate CTC mechanical metamaterial is designed based on ingenious space designs

for higher ultimate torque and stability. Experiments and finite-element simulations are conducted to investigate the performances of the CTC metamaterial. The proposed metamaterial features higher transverse stability and bearing capacity than the original CTC metamaterial. The optimized CTC metamaterial can realize advanced applications in soft robotics, vehicle engineering, and energy technology.

Theoretical calculations illustrate the transmission mechanisms of the overrunning clutch, and the geometrical parameters of the CTC metamaterial and the conical structure are determined based on the calculations. The proposed overrunning clutch features simple construction, and the conical structure has the ability to self-compensate after wear. A drive system is established to verify the validity of the overrunning clutch, and the system exhibits excellent performances under working and overrunning states. The proposed overrunning clutch provides a new one-direction transmission method.

Conflict of interest *On behalf of all authors, the corresponding author states that there is no conflict of interest.*

Author contributions ***Yanbin Wang:*** *Investigation, Conceptualization, Methodology, Writing – original draft.* ***Haifeng Ou:*** *Investigation, Methodology.* ***Lingling Hu:*** *Writing – review & editing, Supervision, Formal analysis, Resources.*

Acknowledgements *This work was supported by the National Natural Science Foundation of China (Grant No. 12172388).*

1 Y. Liu, T. Yang, D. Wang, and Y. Yu, A low-cost single-motor-driven climbing robot based on overrunning spring clutch mechanisms, Int. J. Adv. Robot. Syst. **19**, 172988062210797 (2022).
2 H. Z. Yan, B. Wen, Z. B. Wang, C. Zhu, D. Ni, and M. H. Lin, Wear analysis of support spring of sprag clutch during state of overrunning, Math. Probl. Eng. **2022**, 3417760 (2022).
3 Y. C. Wu, and Z. H. Sun, Design and analysis of a novel speed-changing wheel hub with an integrated electric motor for electric bicycles, Math. Probl. Eng. **2013**, 369504 (2013).
4 A. H. Sakhaei, S. Kaijima, T. L. Lee, Y. Y. Tan, and M. L. Dunn, Design and investigation of a multi-material compliant ratchet-like mechanism, Mech. Mach. Theor. **121**, 184 (2018).
5 K. Liu, and E. Bamba, Analytical model of sliding friction in an overrunning clutch, Tribol. Int. **38**, 187 (2005).
6 M. Controzzi, L. Bassi Luciani, and F. Montagnani, Unified approach to bi-directional non-back drivable roller clutch design, Mech. Mach. Theor. **116**, 433 (2017).
7 H. Zhao, B. Wang, G. Zhang, and J. Li, Concept of a new overrunning clutch with the characteristic of reverse force transfer at high speed, Eng. Rep. **3**, e12415 (2021).
8 C. Huang, M. Liu, and Y. Zhao, An analytical model of multiarc sprag clutch considering geometry and internal interaction during engagement, Shock Vib. **2017**, 2393578 (2017).
9 Y. Xue, Z. Wang, D. Chen, S. Tao, and Y. Lu, Design and test of a new type of overrunning clutch, Machines **10**, 1188 (2022).
10 H. Yang, W. Jiang, M. Li, and L. Ma, Multi-material 3D double-V metastructures with tailorable Poisson's ratio and thermal expansion, Int. J. Mech. Sci. **210**, 106733 (2021).
11 B. Liu, J. Feng, K. Yu, J. Li, Q. Hu, Z. Lin, and J. Fu, Three-dimensional auxetic structure design methods based on bulking-induced deformation and the application in soft crawling robot, Compos. Part B-Eng. **244**, 110146 (2022).
12 G. F. Li, H. T. Liu, Y. B. Wang, and G. B. Cai, Mechanical properties of 3D auxetic structure: Emergence of transverse isotropy, Int. J. Mech. Sci. **250**, 108285 (2023).
13 N. Ma, Q. Han, S. Han, and C. Li, Hierarchical re-entrant honeycomb metamaterial for energy absorption and vibration insulation, Int. J. Mech. Sci. **250**, 108307 (2023).
14 X. Tan, B. Wang, Y. Yao, K. Yao, Y. Kang, S. Zhu, S. Chen, and P. Xu, Programmable Buckling-based negative stiffness metamaterial, Mater. Lett. **262**, 127072 (2020).
15 Y. Liu, F. Pan, F. Xiong, Y. Wei, Y. Ruan, B. Ding, K. Yang, and Y. Chen, Ultrafast shape-reconfigurable chiral mechanical metamaterial based on prestressed bistable shells, Adv. Funct. Mater. **33**, 2300433 (2023).
16 M. Xu, Z. Zhao, P. Wang, Y. Zhang, X. Guo, H. Lei, and D. Fang, Planar bi-metallic lattice with tailorable coefficient of thermal expansion, Acta Mech. Sin. **38**, 421546 (2022).
17 Z. Zhang, X. Zhang, W. Chen, Y. Rasim, W. Salman, H. Pan, Y. Yuan, and C. Wang, A high-efficiency energy regenerative shock absorber using supercapacitors for renewable energy applications in range extended electric vehicle, Appl. Energy **178**, 177 (2016).
18 H. Li, P. Zheng, T. Zhang, Y. Zou, Y. Pan, Z. Zhang, and A. Azam, A high-efficiency energy regenerative shock absorber for powering auxiliary devices of new energy driverless buses, Appl. Energy **295**, 117020 (2021).
19 T. Frenzel, M. Kadic, and M. Wegener, Three-dimensional mechanical metamaterials with a twist, Science **358**, 1072 (2017).
20 M. Fu, F. Liu, and L. Hu, A novel category of 3D chiral material with negative Poisson's ratio, Compos. Sci. Tech. **160**, 111 (2018).
21 L. Zhang, H. Du, and W. Yu, Constitutive modeling of chiral mechanical metastructures, Acta Mech. Sin. **39**, 422342 (2023).
22 S. Wang, C. Deng, O. Ojo, N. Yang, B. Akinrinlola, J. Kozub, and N. Wu, Design and testing of a DNA-like torsional structure for energy absorption, Mater. Des. **226**, 111642 (2023).
23 Y. B. Wang, H. T. Liu, and Z. Y. Zhang, Rotation spring: Rotation symmetric compression-torsion conversion structure with high space utilization, Compos. Struct. **245**, 112341 (2020).
24 Y. Miyazawa, H. Yasuda, and J. Yang, Design of compliant mechanisms for origami metamaterials, Acta Mech. Sin. **39**, 723169 (2023).
25 H. Han, V. Sorokin, L. Tang, and D. Cao, Origami-based tunable mechanical memory metamaterial for vibration attenuation, Mech. Syst. Signal Process. **188**, 110033 (2023).
26 G. Lin, J. Li, P. Chen, W. Sun, S. A. Chizhik, A. A. Makhaniok, G. B. Melnikova, and T. A. Kuznetsova, Buckling of lattice columns made from three-dimensional chiral mechanical metamaterials, Int. J. Mech. Sci. **194**, 106208 (2021).
27 T. Frenzel, V. Hahn, P. Ziemke, J. L. G. Schneider, Y. Chen, P. Kiefer, P. Gumbsch, and M. Wegener, Large characteristic lengths in 3D chiral elastic metamaterials, Commun. Mater. **2**, 4 (2021).
28 L. Qiu, Y. Yu, L. Zheng, and M. Chen, A novel analytical method of windmill chiral cell structure (WCCS), Compos. Struct. **268**, 113973 (2021).
29 Y. Wei, C. Huang, L. Ren, Y. Liang, Z. Wu, and M. Yuan, Topological study about deformation behavior and energy absorption performances of 3D chiral structures under dynamic impacts, J. Strain Anal. Eng. Des. **58**, 208 (2023).
30 W. Xu, Z. Liu, L. Wang, and P. Zhu, 3D chiral metamaterial modular design with highly-tunable tension-twisting properties, Mater. Today Commun. **30**, 103006 (2022).
31 A. Bergamini, M. Miniaci, T. Delpero, D. Tallarico, B. van Damme, G. Hannema, I. Leibacher, and A. Zemp, Tacticity in chiral phononic crystals, Nat. Commun. **10**, 4525 (2019).
32 Y. Zhou, L. Ye, and Y. Chen, Investigation of novel 3D-printed diatomic and local resonant metamaterials with impact mitigation capacity, Int. J. Mech. Sci. **206**, 106632 (2021).
33 H. Zhang, Y. Luo, and Z. Kang, Bi-material microstructural design of chiral auxetic metamaterials using topology optimization, Compos.

Struct. **195**, 232 (2018).
34 W. Chen, D. Ruan, and X. Huang, Optimization for twist chirality of structural materials induced by axial strain, Mater. Today Commun. **15**, 175 (2018).
35 J. I. Lipton, R. MacCurdy, Z. Manchester, L. Chin, D. Cellucci, and D. Rus, Handedness in shearing auxetics creates rigid and compliant structures, Science **360**, 632 (2018).
36 H. Wang, C. Zhang, Q. H. Qin, and Y. Bai, Tunable compression-torsion coupling effect in novel cylindrical tubular metamaterial architected with boomerang-shaped tetrachiral elements, Mater. Today Commun. **31**, 103483 (2022).
37 J. X. Wang, Q. S. Yang, Y. L. Wei, and R. Tao, A novel chiral metamaterial with multistability and programmable stiffness, Smart Mater. Struct. **30**, 065006 (2021).
38 J. Hao, D. Han, X. G. Zhang, X. C. Teng, H. H. Xu, W. Jiang, J. P. Lang, X. H. Ni, Y. M. Luo, H. R. Li, and X. Ren, A novel compression-torsion coupling metamaterial with tunable Poisson's ratio, Constr. Build. Mater. **395**, 132276 (2023).
39 C. Ma, H. Lei, J. Liang, W. Wu, T. Wang, and D. Fang, Macroscopic mechanical response of chiral-type cylindrical metastructures under axial compression loading, Mater. Des. **158**, 198 (2018).
40 Y. B. Wang, H. T. Liu, and D. Q. Zhang, Compression-torsion conversion behavior of a cylindrical mechanical metamaterial based on askew re-entrant cells, Mater. Lett. **303**, 130572 (2021).
41 C. Yang, K. Yang, Y. Tian, M. Fu, and L. Hu, Theoretical analysis on the stiffness of compression-torsion coupling metamaterials, Extreme Mech. Lett. **46**, 101336 (2021).
42 R. Zhong, M. Fu, X. Chen, B. Zheng, and L. Hu, A novel three-dimensional mechanical metamaterial with compression-torsion properties, Compos. Struct. **226**, 111232 (2019).

基于曲面板压扭超材料的新型超越离合器

王彦斌, 欧海峰, 胡玲玲

摘要 超越离合器是一种广泛应用于传动系统的单向驱动机构. 然而, 现有的超越离合器结构复杂, 对制备精度要求高, 并且在一定程度的磨损后失效. 为了解决这些问题, 我们提出了一种由锥形结构和新型曲面板压扭超材料组成的新型超越离合器. 通过理论计算指导了曲面板压扭超材料的材料分布, 保证变形协调, 以获得更大的极限扭矩. 推导了该超越离合器的传动机理, 指导了压扭超材料和锥形结构的参数选择. 实验和有限元仿真结果表明, 曲面板压扭超材料具有优异的压扭转换效率、柔度和横向刚度, 有利于减小超越状态的阻力, 保证运行稳定性. 采用新型超越离合器构建的单向传动系统在工作状态和超越状态下均表现出可靠的性能. 构造的超越离合器提供了一种有效的单向传动方法. 该离合器结构简单, 具有磨损自补偿能力, 在小型化、轻量化设备或机器人领域有很大的应用潜力.